ACS Chemical Neuroscience

Research Article

pubs.acs.org/chemneuro

Voltage-Induced Misfolding of Zinc-Replete ALS Mutant Superoxide Dismutase-1

Yunhua Shi,[†] Mark J. Acerson,[†] Kevin L. Shuford, and Bryan F. Shaw*

Department of Chemistry and Biochemistry, Baylor University, Waco, Texas 76706, United States

Supporting Information

ABSTRACT: The monomerization of Cu, Zn superoxide dismutase (SOD1) is an early step along pathways of misfolding linked to amyotrophic lateral sclerosis (ALS). Monomerization requires the reversal of two post-translational modifications that are thermodynamically favorable: (i) dissociation of active-site metal ions and (ii) reduction of intramolecular disulfide bonds. This study found, using amide hydrogen/deuterium (H/D) exchange, capillary electrophoresis, and lysine-acetyl protein charge ladders, that ALS-linked A4V SOD1 rapidly monomerizes and partially unfolds in an external electric field (of physiological strength), without loss of metal ions, exposure to disulfide-reducing agents, or Joule heating. Voltage-induced monomerization was not observed for metal-free A4V SOD1, metal-free WT SOD1, or metal-loaded WT SOD1. Computational modeling suggested a mechanism for this counterintuitive effect: subunit macrodipoles of dimeric SOD1 are antiparallel and amplified 2-fold by metal coordination, which increases torque at the dimer interface as subunits rotate to align with the electric field.

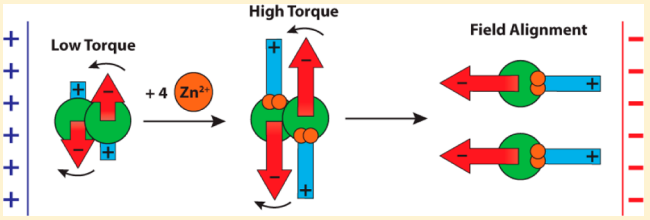

KEYWORDS: *Aggregation, zinc, electric field, SOD1, amyotrophic lateral sclerosis, voltage*

The development of tools to map intracellular electric fields[1] is beginning to suggest that a significant fraction of cytosolic proteins are, like the majority of membrane proteins, exposed to strong electric fields that range in strength from 10^4 to 10^7 V/m.[2] For example, the use of nanoscale photonic voltmeters to measure electric fields emanating from mitochondrial or nuclear surfaces suggests that electric fields extend, as would the field's effect on cytosolic protein structure, to debye lengths >10 nm.[2,3] Historically, the electric fields emanating from cellular or membrane surfaces, which do reach field strengths of 10^7 V/m, were predicted (with Gouy–Chapman theory) to be short-reaching[4] and screened at debye lengths of ∼1 nm. Such predictions have remained unverified because conventional tools (patch-clamp and dye techniques) measure potential at membrane surfaces, not intracellularly.[5,6]

The reasons why intracellular debye lengths might extend beyond 1 nm are unclear, but nonuniform distributions of intracellular K^+ represent one possibility. Potassium is the primary free ion that screens electrostatic interactions inside cells (e.g., in mammalian neurons, intracellular $[K^+]$ = 140 mM, $[Na^+]$ = 5–15 mM, $[Cl^-]$ = 4–30 mM). Fluorescent probes for K^+ have provided the first glimpse of intracellular potassium distributions and suggest that intracellular $[K^+]$ can vary ∼10–30-fold across the interior of cultured cells.[7,8] A subcellular microdomain containing low $[K^+]$ would permit, *ceteris paribus*, longer field propagation than regions with higher $[K^+]$ (e.g., debye lengths would increase 6-fold from $[K^+]_{ave}$ = 140 mM to $[K^+]_{local}$ = 4 mM).

The ability of external electric fields to modulate the structure of integral membrane proteins is a central dogma in voltage gating;[9] however, few studies can be found for field effects on water-soluble proteins.[10,11] Lysozyme and synapse-associated protein 97 are the few examples of water-soluble proteins that have been reported to undergo conformational changes in response to external electric fields.[12,13] These field-induced effects are poorly understood but are attributed to rotational and translational movement of dipolar residues (or domains) in response to external electric fields.

In this article, we used capillary zone electrophoresis (CE), protein charge ladders,[14,15] amide hydrogen/deuterium (H/D) exchange mass spectrometry, native isoelectric focusing, and size exclusion chromatography to study how electric fields of biological strength (10^4 V/m) affect the tertiary and quaternary structures of wild-type (WT) superoxide dismutase-1 (SOD1) and the A4V variant of SOD1. The SOD1 protein is a ubiquitous homodimeric metalloenzyme found in the cytosol,[16] nucleus,[17] lysosome,[18] and mitochondrion.[19] The Ala4Val missense mutation in *SOD1* is causally linked to familial amyotrophic lateral sclerosis (ALS) and is the most commonly occurring ALS-*SOD1* mutation in North America.[20] Amyotrophic lateral sclerosis is a fatal disease characterized by selective death of upper and lower motor neurons,[21] and *SOD1* mutations are hypothesized to cause familial ALS by accelerating SOD1 self-assembly into a neurotoxic oligomer.[22] The aggregation of WT SOD1 has also been causally linked to nonfamilial (sporadic) ALS.[23]

Received: May 22, 2015
Revised: July 9, 2015
Published: July 24, 2015

ACS Publications © 2015 American Chemical Society

DOI: 10.1021/acschemneuro.5b00146
ACS Chem. Neurosci. 2015, 6, 1696–1707

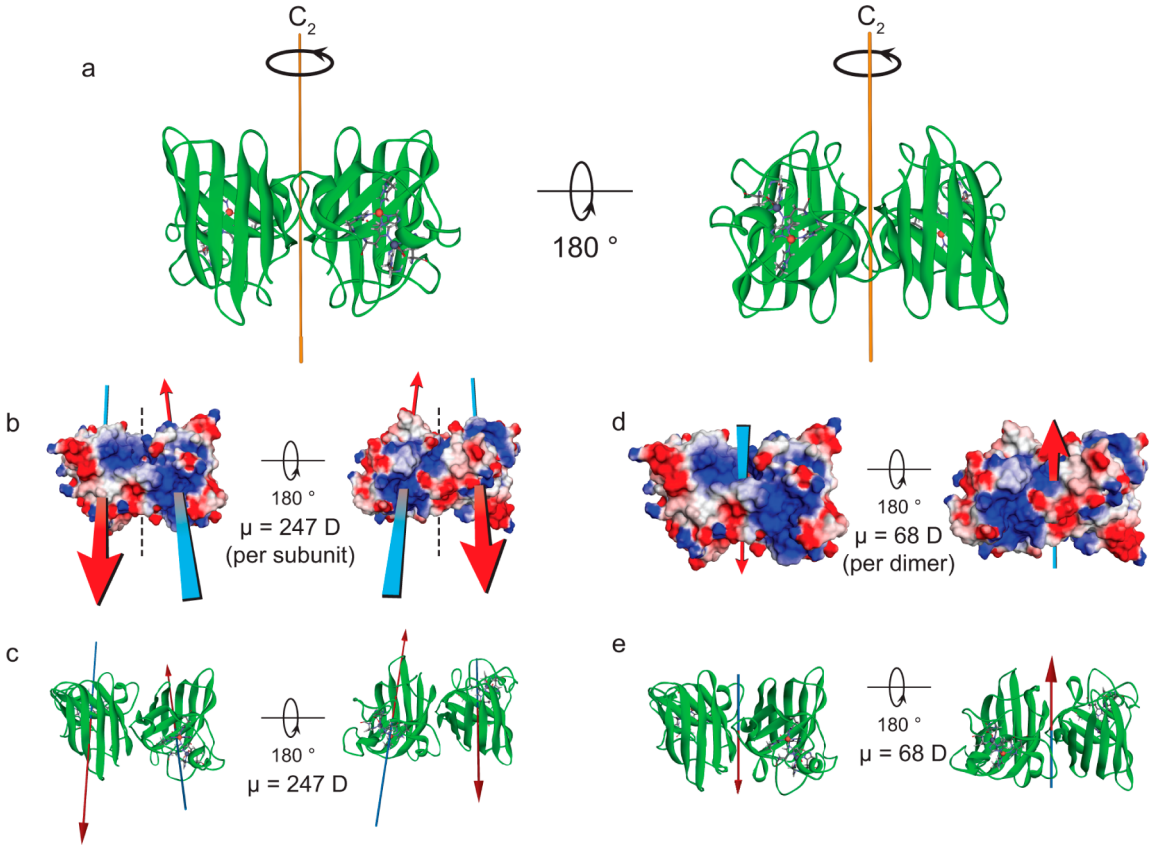

Figure 1. Subunit macrodipoles of WT Cu_2Zn_2–SOD1 are antiparallel and proceed through the metal-binding site. (a) WT Cu_2Zn_2–SOD1 exhibits antiparallel quaternary structure (PDB: 1SOS); C_2 axis of symmetry is indicated with orange line. (b) Electrostatic surface potential of WT Cu_2Zn_2–SOD1: red, negative; blue, positive. Arrows depict direction and magnitude of average dipole moment (μ) for each subunit in units of debye (D): blue, positive; red, negative (PDB: 1SOS). (c) WT Cu_2Zn_2–SOD1 cartoon showing the metal active site, with subunit dipole moment from (b). (d, e) When the SOD1 dimer is treated as a single, continuous polypeptide, the single macrodipole (a vector sum of two subunit macrodipoles) is diminished to 68 D and perpendicular to subunit macrodipoles.

The monomerization of SOD1 has been identified as an early step in the nucleation and propagation of neurotoxic oligomers.[23−27] The dissociation constant (K_d) for dimeric WT SOD1 in its metal-free (apo) state has been measured to be ∼1−10 nM, but it is increased 100-fold by the A4V substitution,[28,29] which occurs at the dimer interface.[20]

Fully metalated SOD1 (WT or A4V), with one Cu^{2+} and Zn^{2+} coordinated per subunit (or two Zn^{2+} per subunit[30]), is a thermostable homodimer (T_m > 70 °C), and its monomerization and unfolding requires, at physiological temperatures, the dissociation of metal ions and reduction of the intramolecular disulfide bond in each subunit.[24,31−33] The current study shows that within electric fields of physiological strength the opposite is true for A4V SOD1: metalation promotes monomerization and unfolding, and it does so at 23 °C. We rationalize the voltage-induced misfolding of A4V SOD1 in terms of the large macrodipoles of each SOD1 subunit, which are (according to theoretical modeling) antiparallel to each other and amplified 2-fold by metal coordination.

RESULTS

We suspected that the quaternary structure of SOD1 (WT or A4V) might be particularly sensitive to external electric fields because subunits of the SOD1 homodimer are situated antiparallel to one another (Figure 1a). To the extent that each subunit exhibits an overall dipole, i.e., a macrodipole,[34,35] that is not parallel with the C_2 rotational axis of the dimer (Figure 1a), then the macrodipoles of each subunit will be oriented antiparallel to one another when populating dimeric states. These antiparallel macrodipoles will generate, in an applied electric field, some degree of destabilizing rotational torque at the dimer interface as each subunit rotates to align its dipole with the external field.

To characterize the electrostatic properties and the macrodipoles of SOD1, solutions to the Poisson−Boltzmann equation were calculated to approximate electrostatic surface potentials based upon a crystal structure of dimeric WT Cu_2Zn_2–SOD1 (Figure 1b). The magnitude and direction of the macrodipole of each subunit were calculated by assigning a partial charge to all atoms in the crystal structure (Figure 1b,c). Macrodipoles were calculated to be 247 D for each subunit of Cu_2Zn_2–SOD1 and were predicted to be antiparallel to one another (Figure 1b,c). Notably, the macrodipole of each Cu_2Zn_2–SOD1 subunit proceeds through the metal binding region (Figure 1b,c); the metal binding site is the positive pole of the macrodipole. When the SOD1 homodimer is treated as a continuous single polypeptide, the subunit macrodipoles do *not* entirely cancel to yield a zero dipole because the subunit macrodipoles are not perfectly antiparallel (Figure 1b−e). Instead, the macrodipole of the entire homodimer, a single macrodipole, is reduced to 68 D and is now parallel to the C_2 rotational axis and perpendicular to the macrodipoles of individual subunits (Figure 1d,e).

DOI: 10.1021/acschemneuro.5b00146
ACS Chem. Neurosci. 2015, 6, 1696−1707

Because the SOD1 protein fluctuates between dimeric and monomeric states, it is reasonable to assume that the macrodipole of SOD1 fluctuates (oscillates) between the single macrodipole of the homodimer shown in Figure 1d and the two antiparallel macrodipoles of individual subunits shown in Figure 1b. Therefore, we believe that it is indeed correct to calculate macrodipoles of homodimeric SOD1 in both the actual homodimeric state, where the SOD1 homodimer is treated as a continuous polypeptide, and the monomeric state, where macrodipoles are calculated for individual polypeptide chains (irrespective of charged groups on the neighboring subunit). Furthermore, the treatment of the SOD1 homodimer as a continuous polypeptide with a single macrodipole (Figure 1d) is reasonable when considering that charged or polarizable groups of one subunit are very close to functional groups in the neighboring subunit. For example, in the crystal structure of WT Cu_2Zn_2−SOD1 (PDB: 2C9V), ε-NH_3^+ of Lys9 on one subunit is 4.3 Å from β-$CONH_2$ of Asn53 on the opposing subunit; β-CO_2 of Asp52 is also 3.8 Å from the β-CH_3 of Val5 on the opposing subunit.

Net Charge of A4V Zn_4−SOD1 Is One-Half of WT Zn_4−SOD1 in an Electric Field. The quaternary structures of A4V and WT apo-SOD1 and Zn_4−SOD1 in an external electric field ($E = 2.5 \times 10^4$ V/m) were assayed by measuring the net charge (Z) of each protein in the external field. The net charge of WT apo-SOD1 was previously determined[15] to be $Z = -12.13 \pm 0.08$ per dimer at pH 7.4 (which is similar to the predicted net charge of $Z = -13.0$). The net charge of WT Zn_4−SOD1 was previously measured to be only $Z = -8.54 \pm 0.12$ per dimer (and not $Z = -4.13$ per dimer, as one might expect upon binding four Zn^{2+}; this disparity is a result of charge regulation).[15] Given these values of net charge for apo-SOD1 and Zn_4−SOD1, the monomerization of either of these proteins would result in, and can be assayed by, a reduction in the magnitude of net charge of 50%, from −12.1 to −6.0 (for apo-SOD1) or −8.5 to −4.2 (for Zn_4−SOD1).

The only convenient, accurate method for measuring the net charge of a protein, which is the method we used, is to synthesize a protein charge ladder of the protein[36] and analyze the charge ladder with capillary electrophoresis. Protein charge ladders are chemical derivatives of a protein, most commonly synthesized by acetylating (neutralizing) lysine-ε-NH_3^+ with acetic anhydride. The relative mobility of each rung of the charge ladder can be used to determine the net charge of the unacetylated protein.[15]

The quaternary structure of the Cu_2Zn_2 state of WT and A4V SOD1 was not examined in this study because properly metalated A4V Cu_2Zn_2−SOD1, where Zn^{2+} and Cu^{2+} are properly coordinated at their respective sites, is difficult to synthesize *in vitro* because the A4V SOD1 protein mis-metalates.[37] Instead, we analyzed the effects of an electric field on the quaternary structure of zinc-replete, disulfide-intact WT and A4V SOD1, where 2 Zn^{2+} ions are bound per subunit (denoted Zn_4−SOD1). Zinc-rich states of SOD1 ($Zn_{\geq 3}$−SOD1) are physiologically relevant.[30]

Prior to synthesis of WT and A4V SOD1 charge ladders, all proteins were analyzed with CE to determine the mobility of the zeroth rung of each ladder, which represents unacetylated SOD1. Both A4V and WT proteins exhibited one predominant peak during capillary electrophoresis, before and after the coordination of 4 equiv of Zn^{2+} per dimer (Figure S1). A4V apo-SOD1 displayed a broader peak than WT apo-SOD1 with a mobility that was ∼0.4 cm^2/(kV min) lower than WT apo-SOD1 (Figure S1a). This lower mobility is likely caused by a greater hydrodynamic drag of A4V apo-SOD1 compared to that of WT apo-SOD1 (not a difference in net charge, as demonstrated below). Coordination of four Zn^{2+} decreased the mobility of WT and A4V compared to that of their apo forms by 1.93 and 2.60 cm^2/(kV min), respectively (Figure S1b), as previously observed for WT SOD1[15] and other ALS variants.[14]

Lysine-acetyl charge ladders of WT and A4V apo- and Zn_4−SOD1 were synthesized by acetylating 1−3 lysine-ε-NH_3^+ (per polypeptide chain) under mild conditions that favor the native state of SOD1 (Figure 2). Apo-SOD1 lysine-acetyl charge ladders were *not* generated by demetalating a zinc-replete lysine-acetyl SOD1 ladder; instead, acetylation of WT and A4V apo-SOD1 occurred after demetalation. Similarly, acetylation of WT and A4V Zn_4−SOD1 was carried out on the Zn_4−SOD1 protein and not by the addition of Zn^{2+} to the lysine-acetyl charge ladder of apo-SOD1. Charge ladders were then extensively characterized (with ICP-MS, and for Co^{2+}-SOD1 ladders, with UV−vis spectroscopy) to demonstrate proper metal binding and the maintenance of native structure after acetylation (previous experiments have validated the use of charge ladders for WT and several ALS-variant SOD1 proteins[14,15]).

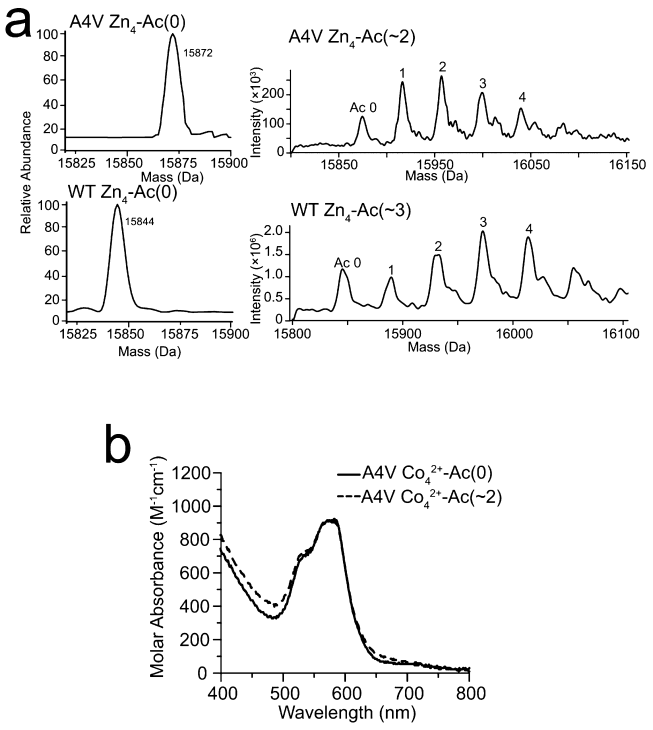

Figure 2. Mass spectrometric and UV−vis characterization of zinc- and cobalt-replete A4V and WT SOD1 before and after synthesis of lysine-acetyl protein charge ladders. (a) Electrospray ionization mass spectra of A4V and WT Zn_4−SOD1 before acetylation (left) and after acetylation (right). The number of acetylated lysine residues, denoted Ac(N), refers to the number of acetyl modifications per monomer (the SOD1 dimer dissociates during electrospray ionization). (b) UV−vis spectra of A4V Co_4−SOD1 before and after acetylation.

Each SOD1 protein charge ladder was analyzed with ICP-MS in order to determine metal content and ensure that acetylation did not result in loss of metal ions (Table S1). Metal analysis showed that ∼4 equiv of Zn^{2+} (per SOD1 dimer) were bound to the zinc-replete derivatives of A4V and WT SOD1 and that

DOI: 10.1021/acschemneuro.5b00146
ACS Chem. Neurosci. 2015, 6, 1696−1707

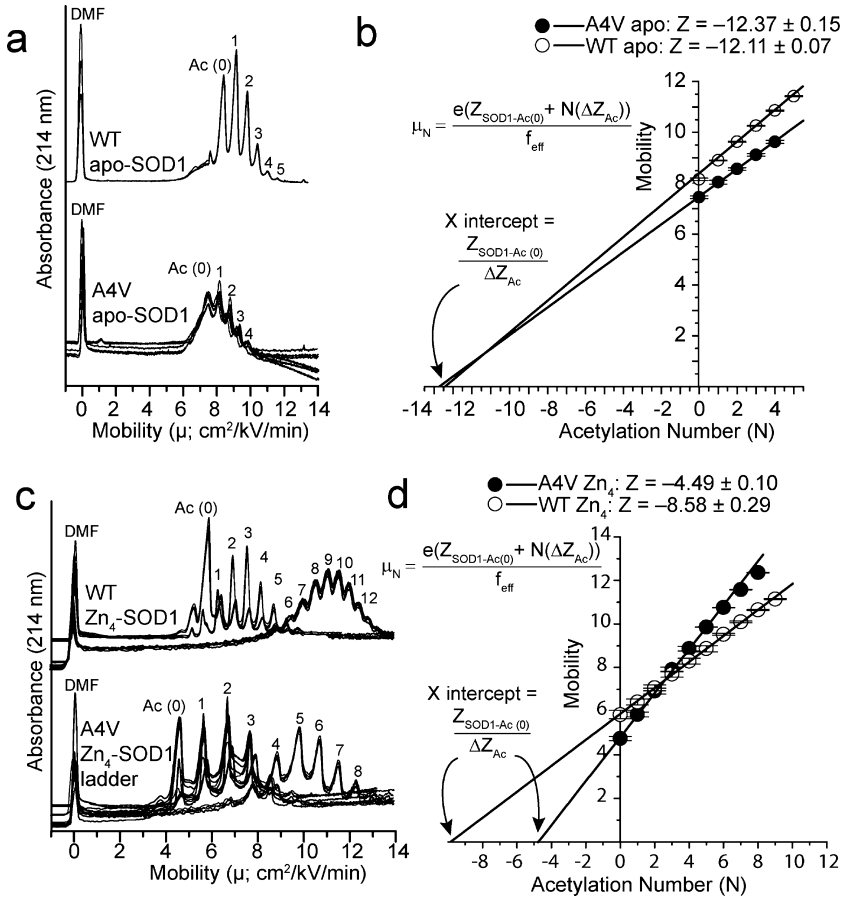

Figure 3. Determination of quaternary structure (i.e., net charge, Z) of A4V and WT Zn_4-SOD1 and apo-SOD1 in a thermally controlled, external electric field (15 kV/60.2 cm, 15 °C, pH 7.4). (a) Electropherograms of protein charge ladders of A4V and WT apo-SOD1. Replicate electropherograms are overlaid to demonstrate reproducibility. Each rung is labeled according to its number of acetylated lysine residues (per dimer, in the case of WT SOD1). The magnitude of each rung is a reflection of the varied amount of acetic anhydride added (to achieve the desired level of modification) and the intrinsic reactivity of surface lysines. (b) Plot of electrophoretic mobility of each rung (μ) vs the number of acetylated lysine corresponding of that rung (N) for protein charge ladders of A4V and WT apo-SOD1. The electrophoretic mobility of each rung can be expressed by the equations shown in (b) and (d), where $Z_{SOD1\text{-}Ac(0)}$ is the net charge of unacetylated A4V or WT SOD1, ΔZ_{Ac} is the change in net charge upon acetylation (~0.9), e represents the charge of an electron, and f_{eff} is the hydrodynamic drag of SOD1 proteins during electrophoresis. The x-intercept of μ vs N is equal to $Z_{SOD1\text{-}Ac(0)}/\Delta Z_{Ac}$. (c) Capillary electrophoresis of protein charge ladders for A4V and WT Zn_4−SOD1. (d) Plot of electrophoretic mobility vs acetylation number for each rung of the protein charge ladders for A4V and WT Zn_4−SOD1. Error bars in (b) and (d) represent standard deviation in mobility values calculated from six replicate measurements.

the content of bound Zn^{2+} did not change significantly after acetylation of WT and A4V Zn_4−SOD1 and transfer from remetalation buffer to electrophoresis buffer (Table S1). For example, ΔZn^{2+}_{Acetyl} = 0.32 ± 0.27 equiv per dimer for A4V Zn_4−SOD1.

Mass spectrometry showed that both zinc-replete and apo A4V and WT SOD1 proteins were pure and not oxidized during metal titrations or acetylation with acetic anhydride (Figure 2a). Cobalt(II) derivatives of SOD1 protein charge ladders were also prepared in order to confirm that acetylated SOD1 proteins were able to bind metal ions at the active site (Co^{2+} is a spectroscopically active coordination analogue for the spectroscopically silent Zn^{2+}).

The binding of Co^{2+} to the active sites of acetylated and unacetylated A4V and WT SOD1 was monitored with UV−vis spectroscopy (Figure 2b). The signature d−d electron absorption band at 450−550 nm indicated that the coordination of metal ions occurred at the active sites in both acetylated and unacetylated WT SOD1. The UV−vis spectra of A4V Co_4−SOD1 and its acetylated derivatives also support the ICP-MS results that show ~4 equiv of Co^{2+} were bound to the active site of acetylated A4V apo-SOD1, assuming the previously estimated molar extinction coefficient of 240 M^{-1} cm^{-1} per bound Co^{2+} (Figure 2b).[15] The binding of metal ions to the active site of acetylated WT and A4V SOD1, and retention of metal ions by the charge ladders, is consistent with previous analyses of Co_4−SOD1 charge ladders for WT SOD1 and other ALS variants with UV−vis and ICP-MS.[14,15]

The net charge of apo- and Zn_4−SOD1 in the external electric field was calculated by plotting the mobility of each rung versus its number of acetylated residues (Figure 3). The x-intercept of this plot (Figure 3b,d) is proportional to the net charge of each unacetylated protein, denoted $Z_{SOD1\text{-}Ac(0)}$, divided by the change in net charge associated with each acetylation, denoted ΔZ_{Ac}. The identity (mobility) of the zeroth rung of the ladder, which represents the unacetylated protein, was verified by (i) comparison to the electropherogram of the pure, unacetylated protein (Figure S1), (ii) analysis of lysine-acetyl charge ladders with ESI-MS (Figure 2a), and (iii) by spiking the charge ladder with an aliquot of the unacetylated protein to deliberately increase the intensity of the zeroth rung during CE (Figure 3a,c).

DOI: 10.1021/acschemneuro.5b00146
ACS Chem. Neurosci. 2015, 6, 1696−1707

In the external electric field, A4V apo-SOD1 exhibited a net charge of −12.37 ± 0.15 (Figure 3a,b, Table S2) which is indistinguishable from the measured net charge of WT apo-SOD1 in the external field, i.e., $Z = -12.11 \pm 0.07$ (Figure 3a,b, Table S2). These values of net negative charge are consistent with the predicted net charge of dimeric apo-SOD1 (WT or A4V) of $Z = -13$. Thus, the measured net charge of WT and A4V apo-SOD1 indicates that these proteins are both dimeric, even in the presence of an electric field of 2.5×10^4 V/m (and that each protein remains dimeric after the acetylation of a few lysine residues). If either of the two apo proteins was monomeric, then we would have observed values of net charge of $Z \approx -6$. For example, the net charge of monomeric WT apo-SOD1 (prepared by reducing intramolecular disulfide bonds in apo-SOD1) has been previously measured to be $Z = -6.92 \pm 0.14$.[15]

The WT Zn_4−SOD1 protein exhibited, in the external electric field, a net charge of −8.58 ± 0.29 at pH 7.4 (Figure 3c,d, Table S2), which is consistent with our previous measurement of $Z = -8.54 \pm 0.12$ for WT Zn_4−SOD1.[15] We reiterate that the binding of 4 Zn^{2+} to WT SOD1 decreases the net charge by ∼4 units instead of ∼8 units, as previously observed,[15] because of an inexplicably large degree of charge regulation. The A4V Zn_4−SOD1 has, in contrast, a net charge of $Z = -4.49 \pm 0.10$ (Figure 3c,d, Table S2). The diminished magnitude of net charge of A4V Zn_4−SOD1, by 52% compared to that of WT Zn_4−SOD1, suggests that the A4V Zn_4−SOD1 protein existed as a monomer (and is more accurately described as 2[Zn_2−SOD1] or Zn_2−SOD1). Additional control experiments were performed (described below) to demonstrate that A4V Zn_4−SOD1 was dimeric before exposure to the external field.

The low magnitude of net charge of A4V Zn_4−SOD1, compared to that of WT Zn_4−SOD1, was not the result of random or systematic experimental error such as mishandling or inadvertent denaturation of the unstable A4V protein. The net charge of A4V Zn_4−SOD1 in the electric field was observed repeatedly with two batches of A4V SOD1 protein that were separately expressed, purified, demetalated, and remetalated with Zn^{2+}.

Although the net charge of A4V and WT Zn_4−SOD1 proteins will differ 2-fold depending upon its state of dimerization, their pI's will be independent (largely) of quaternary structure.[15] Therefore, WT and A4V Zn_4−SOD1 proteins were analyzed with native IEF to determine if the net charge of A4V Zn_4−SOD1 is half that of WT Zn_4−SOD1 in the external field because of monomerization or, in contrast, because the A4V substitution altered the pK_a of multiple ionizable groups via structural perturbation (which only coincidentally resulted in a decreased net charge of ∼50%). Both A4V and WT Zn_4−SOD1 proteins exhibited pI = 5.2 (Figure S2). Thus, the A4V substitution does not change the intrinsic net charge of the SOD1 polypeptide. We conclude that A4V Zn_4−SOD1 monomerized in the electric field because the net charge of A4V Zn_4−SOD1 is half that of WT Zn_4−SOD1, without a concomitant difference in the intrinsic net charge of each polypeptide, i.e., $pI_{WT} \approx pI_{A4V}$. WT apo-SOD1, A4V apo-SOD1, and WT Zn_4−SOD1 were, in contrast, dimeric, based upon net charge.

The net charge of A4V Zn_4−SOD1 (actually, 2[Zn_2−SOD1]) in the field also provides information on the number of Zn^{2+} ions that remain coordinated to monomeric A4V SOD1 in the electric field. If metal ions dissociate from A4V Zn_4−SOD1 after monomerization, then the net charge of the A4V monomer would be one-half that of WT apo-SOD1) and not (as it is) one-half the net charge of WT Zn_4−SOD1. Thus, we conclude that two Zn^{2+} ions remain bound to A4V SOD1 after monomerization in the electric field.

Effect of Acetylation on Stability of WT and A4V Zn_4−SOD1. We do not suspect that the monomerization of A4V Zn_4−SOD1 occurred in the electric field because the dimer was destabilized by the acetylation of 1−3 lysines per subunit. Numerous studies have shown that the acetylation of lysine residues has minimal effects on the conformation of WT or ALS-variant SOD1.[14,15,38] Moreover, monomerization of A4V apo-SOD1 was not observed in this study or in previous studies of acetylated WT and A4V apo-SOD1 and was not previously observed for acetylated forms of other ALS-variant apo-SOD1 proteins.[14,15,38]

Nevertheless, amide H/D exchange and differential scanning calorimetry (DSC) were performed to confirm that the acetylation of a few lysine residues (∼1−3 residues per monomer) did not alter the thermostability and structure of WT and A4V Zn_4−SOD1 proteins. The similar number of unexchanged hydrogens for each acetyl derivative of either A4V or WT Zn_4−SOD1 during the 60 min H/D exchange experiment, prior to the application of the external field (Figure 4a), suggested that acetylation of lysine residues does not significantly alter the overall structure of either protein. Acetylation actually slowed amide H/D exchange in A4V Zn_4−SOD1, resulting in a slight increase in the number of unexchanged hydrogens (4 H's per monomer in Ac (4) compared to Ac (0)). This slowing of H/D exchange upon acetylation does not suggest, as one might assume, that acetylation actually stabilized native SOD1 (or increased its thermostability). Instead, the protective effect of lysine acetylation against amide H/D exchange,which has been previously observed for several proteins including WT and ALS-variant SOD1, myoglobin, and carbonic anhydrase II, has been shown to be electrostatic, not structural, in nature.[14,15,39,40]

The minimal effect of acetylation on the structure of WT and A4V Zn_4−SOD1 was further confirmed with DSC. Prior to acetylation, A4V Zn_4−SOD1 exhibited a T_m value of 68.97 °C, and after acetylation, A4V Zn_4−SOD1 exhibited a T_m of 65.89 °C (Figure 4b); WT Zn_4−SOD1 exhibited a T_m = 76.67 °C before acetylation and T_m = 73.51 °C after acetylation (Figure 4c). The $\Delta T_m = -3.08$ °C upon acetylation of A4V Zn_4−SOD1 is similar to the $\Delta T_m = -3.16$ °C for WT Zn_4−SOD1 upon acetylation. These small decreases in T_m suggest that acetylation does not significantly alter the structure of either A4V or WT Zn_4−SOD1. The ability of A4V Zn_4−SOD1 to remain globular (folded) and thermostable after the acetylation of a few lysine residues per dimer demonstrates that the apparent monomerization of A4V Zn_4−SOD1 in the external field (and the dimerization of A4V apo-SOD1) is caused by the combined effects of the A4V substitution and the coordination of metal ions, not by lysine acetylation.

A4V Zn_4−SOD1 Is Dimeric at 0 kV. Despite the presence of the dimer-destabilizing Ala-to-Val substitution, previous analyses of A4V SOD1 in different states of metalation (including the disulfide-intact apo state) has demonstrated that A4V SOD1 retains its dimeric quaternary structure outside of external electric fields (except of course in the disulfide-reduced apo state, where all SOD1 proteins, WT or mutant, are also monomerized).[32,41−43] In order to confirm the dimeric

DOI: 10.1021/acschemneuro.5b00146
ACS Chem. Neurosci. 2015, 6, 1696−1707

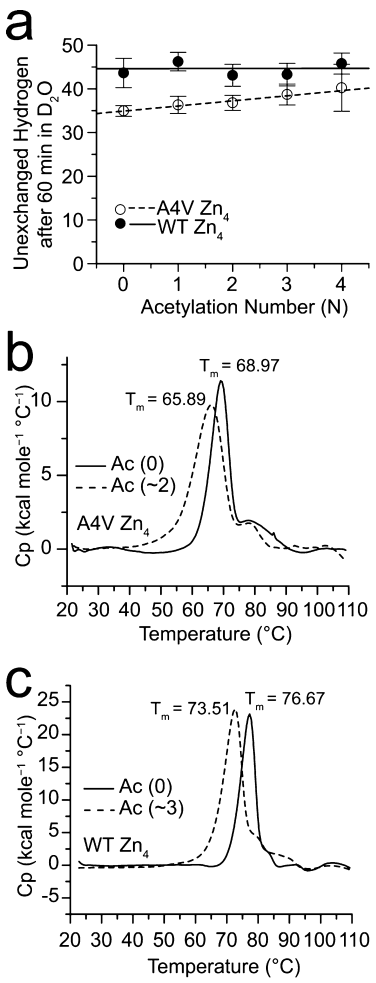

Figure 4. Effect of acetylation (synthesis of protein charge ladders) on the structure and thermostability of A4V Zn_4–SOD1 in the absence of an external electric field. (a) Number of unexchanged amide hydrogens in A4V and WT Zn_4–SOD1 after 60 min in D_2O as a function of the number of acetylated lysines per monomer. (b) DSC of A4V Zn_4–SOD1 before and after acetylation. (c) DSC of WT Zn_4–SOD1 before and after acetylation. The number of acetylated lysine residues is listed per monomer.

quaternary structure of A4V and WT Zn_4–SOD1 in the absence of an electric field, we analyzed both proteins with size exclusion chromatography. The retention time of unacetylated A4V and WT Zn_4–SOD1 was within 0.88 ± 0.01 min of one another, which is consistent with the elution time for the 31.6 kDa homodimer (Figure S3a–d). Elution times were calibrated to molecular weight using a mixture of bovine serum albumin, human Cu_2Zn_2-superoxide dismutase (isolated from human erythrocytes), myoglobin, ubiquitin, and cytochrome c (Figure S3e).

As a control, we analyzed monomeric forms of WT and A4V apo-SOD1 with SEC-HPLC in the absence of an external field. These WT and A4V protein samples were monomerized by reduction of the intramolecular disulfide bonds with 10 mM TCEP (again, disulfide reduction induces monomerization of apo-SOD1[24]). Monomeric SOD1 proteins eluted 3 min later than dimeric forms, with similar elution times to that of myoglobin (16.9 kDa), which was added as an internal standard (Figure S3a–d).

The elution times of acetylated WT and A4V Zn_4–SOD1 demonstrate that acetylation of lysines did not abolish the dimeric state of either WT or A4V Zn_4–SOD1 (Figure S3b,d); acetylated Zn_4–SOD1 (WT or A4V) is dimeric outside of the electric field. In fact, the acetylation of surface lysine residues on WT and A4V Zn_4–SOD1 decreased elution time by only 0.19 and 0.27 min, respectively, during HPLC-SEC (Figure S3b,d). This small change in retention might be caused by electrostatic interactions between SOD1 and zirconium-modified silica, which might be partially anionic due to unreacted silanol groups.[44]

Acceleration of Amide H/D Exchange in A4V Zn_4–SOD1 by an External Electric Field. To further confirm and characterize the change in quaternary structure of A4V Zn_4–SOD1 in response to the external electric field (and to detect possible changes in secondary and tertiary structures), we measured the rate of amide H/D exchange for A4V Zn_4–SOD1 before and after the application of the external electric field. Amide H/D exchange was measured on a 250 μL aliquot of D_2O/A4V Zn_4–SOD1 solution that was contained in the CE reservoir in which the negative electrode was immersed (Figure S4). With the rate of electroosmotic flow in this apparatus (0.3 μL/min), the majority of protein in the CE reservoir (>90%) from which aliquots were removed and analyzed with ESI-MS never passed through the fused silica capillary. Thus, whatever changes we observe in the rate of H/D exchange of proteins will not be caused by protein–silica interactions.

Prior to application of the external electric field, WT and A4V Zn_4–SOD1 proteins were incubated in D_2O for 60 min at 0 kV (Figure 5a). This hour-long preincubation in D_2O allowed the rate of amide H/D exchange to plateau before the application of the external field, thereby leaving only solvent-inaccessible or strongly H-bonded amide NH's unexchanged with D_2O. If these unexchanged amide hydrogens become exposed to D_2O through monomerization of A4V Zn_4–SOD1 (upon application of the electric field), then the number of unexchanged hydrogens should decrease (and the mass of SOD1 should increase) as the amide NH's that were once buried become available for rapid exchange with D_2O.[45] For example, a previous study of WT apo-SOD1 with amide H/D exchange demonstrated that the monomerization of WT apo-SOD1 (via disulfide reduction with dithiothreitol) resulted in the exchange of ~10 additional amide NH's, compared to that with disulfide-intact, dimeric WT apo-SOD1.[45] In this same study, the disulfide reduced A4V apo-SOD1 monomer was determined to be intrinsically disordered and rapidly exchanged all amide NH's with D_2O.[45]

The mass spectra of A4V and WT Zn_4–SOD1 proteins in H_2O (before and after the application of the electric field) show that the protein is pure and not covalently modified (e.g., oxidized) as a result of the electric field. The minor approximately +23 Da modification observable in spectra (before and after the application of the field, Figure 5a,b) likely represents a gas-phase Na^+ adduct.

Mass spectrometry demonstrated that the rate of amide H/D exchange in A4V Zn_4–SOD1 was accelerated by an external electric field (15 kV/60.2 cm), whereas the rate of H/D exchange of WT Zn_4–SOD1 was unaffected by the field (Figure 5c). For example, A4V Zn_4–SOD1 retained ~40 unexchanged NH's (that were protected from H/D exchange with D_2O) prior to application of the electric field (Figure 5c). This number of unexchanged hydrogens in A4V Zn_4–SOD1 decreased by ~4 after 5 min in the electric field (Figure 5c) and continued to decrease (sigmoidally) by ~33 over the next 30 min in the external field. After 30 min in field, only ~5 amide

DOI: 10.1021/acschemneuro.5b00146
ACS Chem. Neurosci. 2015, 6, 1696–1707

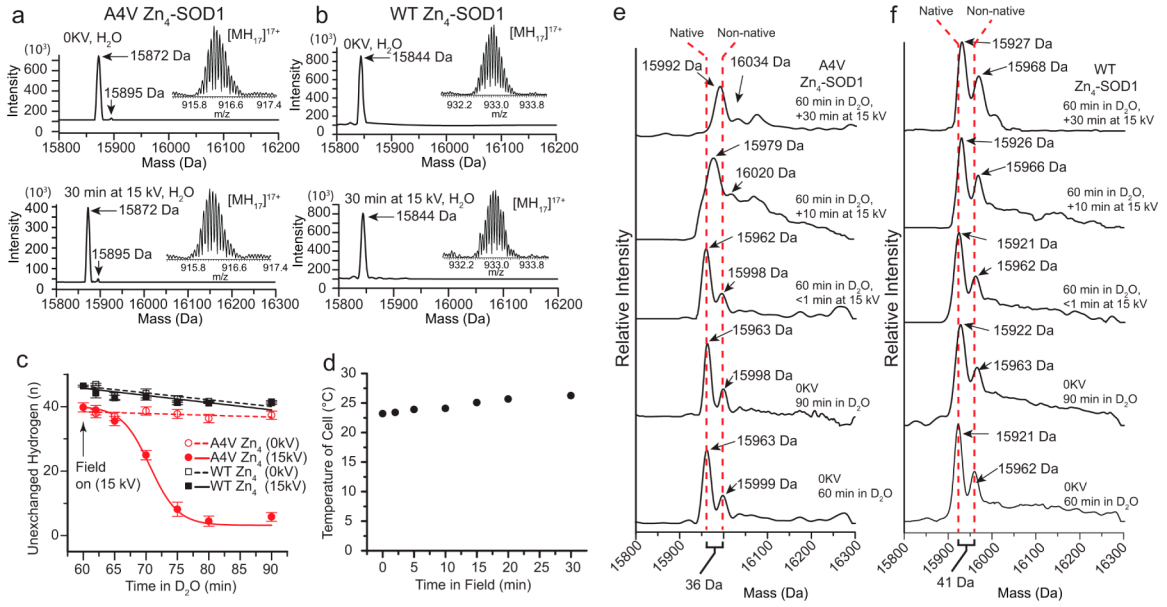

Figure 5. Effect of external electric field (15 kV/60.2 cm) on rate of H/D exchange of WT and A4V Zn_4–SOD1. WT and A4V Zn_4–SOD1 underwent hydrogen/deuterium exchange in 90% D_2O at room temperature for 60 min before application of an external electric field. (a) Representative mass spectra (inset shows raw spectra of $[MH_{17}]^{+17}$ ion) of A4V Zn_4–SOD1 in H_2O before application of electric field (top) and in H_2O after 30 min exposure to electric field (bottom). (b) Similar raw and deconvoluted mass spectra as in part (a) but for WT Zn_4–SOD1. (c) Plot of the number of unexchanged hydrogens in A4V Zn_4–SOD1 and WT Zn_4–SOD1 as a function of time in D_2O. Arrows indicate the time at which the field was applied to WT Zn_4–SOD1 (closed black boxes) and A4V Zn_4–SOD1 (closed red circles); open red circles and open black boxes denoted H/D exchange for WT and A4V Zn_4–SOD1, respectively, without external field (0 kV). (d) Temperature plot of the glass vial containing SOD1 solutions as a function of time over which voltage was applied. (e, f) Representative mass spectra of A4V Zn_4–SOD1 and WT Zn_4–SOD1 after 60–90 min in D_2O without electric field (bottom two spectra) followed by <1–30 additional minutes in D_2O while exposed to the electric field (top three spectra). Red dashed lines designate mass values corresponding to native SOD1 and non-native SOD1.

NH's in A4V Zn_4–SOD1 remained protected from H/D exchange (Figure 5c). In the case of WT Zn_4–SOD1, ~48 unexchanged hydrogens remained before the application of the electric field; however, this number was reduced by only ~6 hydrogens over 30 min in the field (Figure 5c). After 30 min in field, WT Zn_4–SOD1 retained ~40 amide NH's, suggesting that the external electric field did not disrupt the hydrophobic core of WT Zn_4–SOD1 and had a minimal effect on the structure of WT Zn_4–SOD1.

The rapid exchange of most amide NH's in zinc-replete A4V SOD1 suggested that this protein lacked most of its 2°, 3°, and 4° structure. The A4V Zn_2–SOD1 monomer cannot be entirely denatured when exposed to the electric field, however, because (i) ~5 amide NH's remained unexchanged at t = 30 min in field and (ii) the net charge of zinc-replete A4V SOD1 suggests that two Zn^{2+} ions are still coordinated to each chain. If the A4V monomer was in fact fully demetalated and denatured in the electric field, then, as discussed above, the net charge would have been more negative and approximate to half that of dimeric A4V apo-SOD1 ($Z = {}^1/_2\, Z_{\text{A4V apo-SOD1}} = -6.1$) and not half that of dimeric WT Zn_4–SOD1. Thus, because Zn^{2+} cations appear to be bound to monomeric A4V SOD1, there must remain some degree of residual structure that is capable of coordinating two Zn^{2+} ions. Therefore, the monomeric A4V Zn_2–SOD1 protein is best described as predominantly unfolded or misfolded and metalated with two Zn^{2+} per polypeptide chain. The small amount of residual structure (e.g., 5 unexchanged amide NH's) that seems to remain in monomeric A4V Zn_2–SOD1 is in contrast to the intrinsically disordered A4V apo-$SOD1^{2SH}$ monomer observed in previous studies.[43,45,46]

The electric current that is generated during capillary electrophoresis can cause a significant amount of heat (Joule heating) in the capillary and, to a lesser degree, in the corresponding solvent reservoirs. This heat could thermally denature (partially or completely) SOD1 proteins. However, the CE instrument that we used for electrophoresis, and also used to establish the external electric field for H/D exchange experiments, is equipped with a liquid-jacketed capillary that is maintained at 15 °C in order to eliminate the effects of Joule heating. Amide H/D exchange experiments were also carried out in glass reservoirs at room temperature, i.e., > 30 °C *below* the melting transition temperature (T_m) of A4V Zn_4–SOD1 and WT Zn_4–SOD1 that were determined in this study (Figure 4b,c) and previous studies.[47] In addition, the variation in temperature of the D_2O/SOD1 solution in each glass reservoir was monitored throughout the course of the H/D exchange experiment and application of the external field and varied only <3 °C during the course of experiments (Figure 5d). Therefore, it is unlikely that the monomerization of A4V Zn_4–SOD1 was caused by Joule heating during capillary electrophoresis or during the amide H/D exchange experiments. Moreover, if Joule heating was causing monomerization of A4V Zn_4–SOD1, then we would expect to also observe the monomerization of A4V and WT apo-SOD1, whose T_m values are lower than A4V Zn_4–SOD1 (according to previous measurements[46]).

Deconvoluted mass spectra of WT and A4V Zn_4–SOD1 in D_2O, collected before and after exposure to the electric field, are shown in Figure 5e,f. The mass spectra of deuterated samples of WT and A4V Zn_4–SOD1, collected before application of the external field, contain a large satellite peak that is ~36–41 Da greater than the predominant peak in the spectra (bottom-most spectra in Figure 5e,f). This heavier peak

DOI: 10.1021/acschemneuro.5b00146
ACS Chem. Neurosci. 2015, 6, 1696–1707

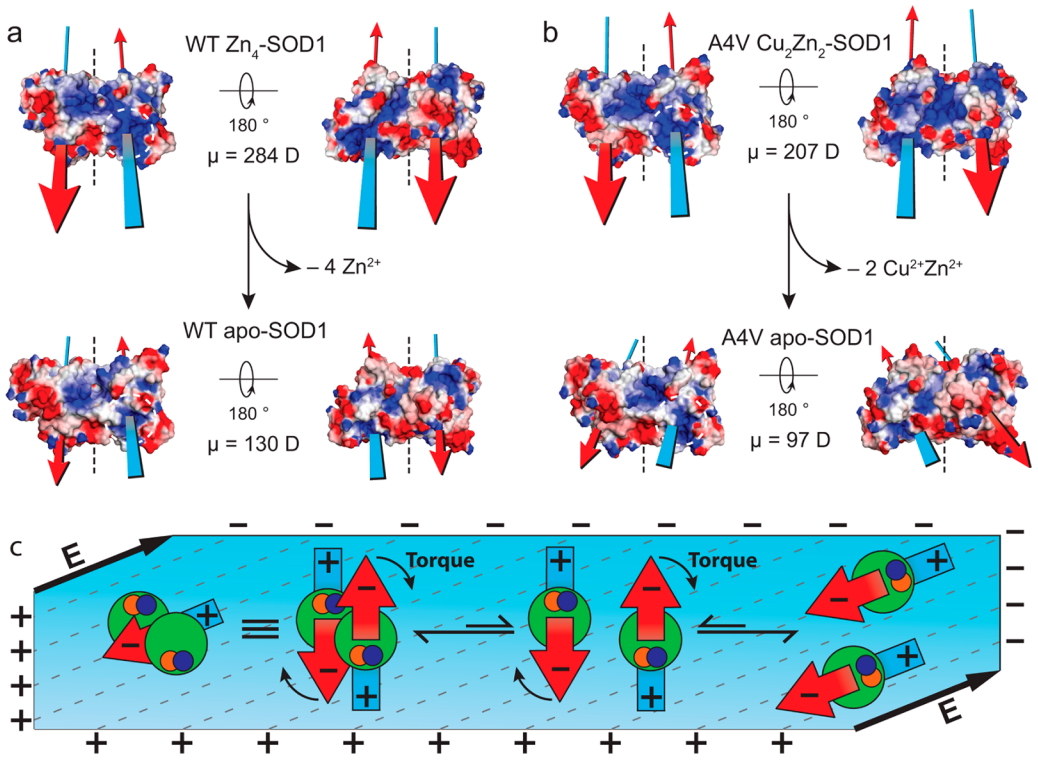

Figure 6. Metal binding amplifies the antiparallel subunit macrodipoles of WT and A4V SOD1. (a) WT Zn_4–SOD1 (PDB: 2C9S) and WT apo-SOD1 (PDB: 1SOS) electrostatic surface potentials calculated using the CHARMm force field and Delphi default template in Discovery Studio 4.1. An average dipole moment (μ) per monomer was calculated from all subunits contained in the crystal structure. This average dipole moment is depicted as a blue–red arrow (blue, positive; red, negative for both electrostatic surface potential and dipole moment). A white, dashed circle designates the metal binding pocket, and a black, dashed line indicates the dimer interface. (b) Same analysis as in (a) except for A4V Cu_2Zn_2–SOD1 (PDB: 1UXM) and A4V apo-SOD1 (PDB: 1UXM). Note that, due to the disordered loops in apo-SOD1, potentials were estimated for apo-SOD1 using the crystal structure of Cu_2Zn_2–SOD1 after removal of the metal ions *in silico*. (c) Proposed mechanism of monomerization for A4V Zn_4–SOD1 in an external electric field. Macrodipoles are represented by arrows, and metalated proteins, by green circles. The triple bar indicates the material equivalence between SOD1 dimers that possess large antiparallel macrodipoles for each subunit (right side of triple bar) or a single, smaller macrodipole when the homodimer is treated as a single polypeptide (left side of triple bar).

is not present in H_2O samples of WT and A4V Zn_4–SOD1 and has been observed in previous studies of WT and A4V SOD1 with amide H/D exchange.[45,46] This peak likely represents SOD1 proteins that populated denatured (or partially denatured) states sufficiently to become nearly perdeuterated. After 30 min at 15 kV/60.2 cm, this peak (whose mass is only ~5 Da lower than that of perdeuterated SOD1) becomes the predominant peak in the spectrum of A4V Zn_4–SOD1, but it remains a minor peak in WT Zn_4–SOD1 (topmost spectra in Figure 5e,f). The predominance of this peak in the spectra of A4V Zn_4–SOD1 suggests that the majority of A4V Zn_4–SOD1 proteins populated non-native (nearly unfolded) states in the electric field. We do not, however, describe the A4V Zn_4–SOD1 protein, in field, as completely unfolded because of the ~5 residual unexchanged amide NH's and the apparent coordination of two Zn^{2+} per polypeptide. In contrast, the low intensity of the heavier peak in the spectra of WT Zn_4–SOD1 suggests that the majority of WT Zn_4–SOD1 proteins populated native states in the electric field.

Computational Analysis of SOD1 Electrostatics. We hypothesize that the macrodipole of each SOD1 subunit will, in an electric field, generate some degree of destabilizing, rotational torque between subunits at the dimer interface, as each subunit must either (i) align its macrodipole to be parallel with the external field and populate monomeric states or (ii) align its dipole to be antiparallel with an adjoining SOD1 subunit (and be antiparallel to the field) in order to populate dimeric states.

We hypothesize that A4V Zn_4–SOD1 populated monomeric states in the electric field because bound metal ions intensified the macrodipole of each subunit and induced rotational torque that was sufficient to disrupt the weakened dimer interface of A4V SOD1 (Figure 6c), whereas the WT Zn_4–SOD1 protein, with its stronger dimer interface, was able to withstand (or overcome) any type of intersubunit rotational torque caused by the external electric field. We predict that coordination at the active site of SOD1 would intensify each subunit's macrodipole because the positive end of the macrodipole of each SOD1 subunit proceeds through the metal binding region (Figure 1b,c).

Predicting the magnitude (and direction) of subunit dipoles and predicting the surface potential for apo-SOD1 are difficult (for WT or A4V) because the metal binding loops of SOD1 become intrinsically disordered in the apo state and the structure of these loops is not observable with X-ray crystallography.[20] To overcome this shortcoming, we calculated the macrodipoles (and electrostatic surface potentials) of apo-SOD1 by removing metal ions (*in silico*) from crystal structures of dimeric WT and A4V Cu_2Zn_2–SOD1 and WT Zn_4–SOD1 (Figure 6a,b, Table S3). Thus, the macrodipole that we calculate for apo-SOD1 subunits is valid only for apo proteins whose loops happen to adopt a structure (during stochastic

DOI: 10.1021/acschemneuro.5b00146
ACS Chem. Neurosci. 2015, 6, 1696–1707

fluctuation) that is similar to the WT and A4V Cu_2Zn_2−SOD1 (or WT Zn_4−SOD1) crystal structures that were used for calculations.

Calculations of the electrostatic surface potential of A4V Cu_2Zn_2−SOD1, WT Zn_4−SOD1, and apo (*in silico*) A4V and WT SOD1, derived from respective crystal structures, showed a large patch of positive surface potential covering the metal coordination site of each subunit (loops IV and VII), the largest positive patch on the surface of SOD1, and, in contrast, a large patch of negative and neutral surface potential at the opposite end of the subunit at β2, β3, and β6 (Figure 6a,b). The calculated macrodipole for each subunit passes directly through the positively charged metal binding region and, oppositely, through β2, β3, and β6 (Figure 6a,b). The macrodipoles of each subunit in WT Cu_2Zn_2−SOD1, WT Zn_4−SOD1, and A4V Cu_2Zn_2−SOD1 were reduced in magnitude (by approximately 2-fold) by the *in silico* removal of all Cu and Zn cations from each active site (Figure 6; Table S3). For these calculations, we used the crystal structure of zinc-replete WT SOD1 (Zn_4−SOD1) and the copper−zinc-replete structure of A4V SOD1 (Cu_2Zn_2−SOD1), as the crystal structure of zinc-replete A4V SOD1 is not available (Figure 6).

The computational prediction that the removal of metal ions reduces the magnitude of the macrodipole of A4V and WT SOD1 (by 2-fold) is intuitive when considering that the positive end of the macrodipole of an SOD1 subunit passes through the metal binding region (Figure 1a−c). Consequently, the binding of metal ions to both A4V and WT SOD1 increases the positive surface potential of a region that is already highly positively charged (Figure 6a,b).

DISCUSSION

The primary observation of this study, that A4V Zn_4−SOD1 monomerized and partially unfolded in an external electric field of 10^4 V/m while A4V apo-SOD1 remained dimeric, is contrary to the conventional wisdom for SOD1. For example, previous studies have shown that the active-site coordination of metal ions to SOD1 increases the stability of dimeric WT and ALS-variant SOD1.[31,32] The results of this study show that the opposite is true in an external electric field, at least in the case of A4V Zn_4−SOD1. Indeed, we would have never predicted that Zn^{2+} ions could assist in the monomerization of A4V SOD1, and we observed this result serendipitously (initially) while attempting to use protein charge ladders to determine if the A4V substitution could alter the intrinsic net charge of SOD1. Ironically, the results of this study do confirm our original suspicion that the Ala4Val missense mutation can reduce the net electrostatic charge of SOD1, albeit by a mechanism different than we expected, monomerization, instead of pK_a perturbation, but nevertheless it did so by a magnitude larger than we expected.

Thus far, A4V Zn_4−SOD1 is the only variant that we have observed to undergo monomerization in an electric field.[14] Our previous analysis of the net charge of other ALS mutant SOD1 proteins (D90A, G93R, and E100K Zn_4−SOD1) demonstrated that these proteins are dimers[14] when exposed to electric fields up to 5.0×10^4 V/m. The exclusivity of the observation for A4V SOD1 does not diminish its potential clinical significance: the A4V mutation accounts for ∼50% of ALS-linked *SOD1* mutations in North America and is associated with a particularly aggressive ALS phenotype[48] compared to that of other ALS-linked missense mutations in *SOD1*.[49]

We hypothesize that the hydrophobic forces joining the two subunits of the relatively weak A4V Zn_4−SOD1 dimer could not withstand the rotational torque produced by antiparallel macrodipoles, in the field of $E = 2.5 \times 10^4$ V/m, whereas WT Zn_4−SOD1, with its stronger dimer interface, was able to resist (or overcome) the rotational torque and thus populated dimeric states. Following this reasoning further, we predict that both WT and A4V apo-SOD1 proteins remained dimeric in the field because each experienced reduced torque as a consequence of the 2-fold smaller macrodipole of each apo subunit (Figure 6a−c).

The presence of strong electric fields, either external fields, generated by mitochondrial, nuclear, or plasma membrane surfaces, or even internal fields, generated by a protein's own charged functional groups, is typically ignored when exploring how missense mutations affect the structure, dynamics, and function of proteins. In fact, only recently has the *internal* electric field of an enzyme been recognized to promote rapid catalysis by long-range polarization of substrates (via the Stark effect).[50] The strength of the external electric fields in this study are by no means biologically unrealistic or stronger than fields emanating from the surface of an axonal membrane of a motor neuron (i.e., at the surface of nodes of Ranvier) or at mitochondrial membrane surfaces, where $E = 10^6$−10^7 V/m.[51,52]

Interactions between SOD1 and membrane surfaces are suspected to play a key role in SOD1 aggregation and ALS pathogenesis. For example, the occurrence of aggregated SOD1 on the surface (and inside) of mitochondria is one hallmark of SOD1-linked ALS.[53−56] Within a myelinated motor neuron, we predict that the SOD1 protein has a higher probability of encountering strong fields emanating from mitochondrial membranes than from plasma membrane surfaces at nodal or synaptic regions. Although the local fields that exist at mitochondrial membranes are known to affect the structure of voltage-gated mitochondrial membrane proteins,[57] local voltage might also be sufficient to alter the structure of SOD1 proteins that are temporarily proximal to mitochondrial membranes, either during transient interactions or during import of SOD1 into mitochondria.

METHODS

WT and A4V SOD1 Isolation, Demetalation, and Remetalation with Zn^{2+}. Wild-type and A4V SOD1 proteins were recombinantly expressed in yeast and purified as previously described.[15] In order to achieve monodisperse and discrete states of zinc metalation, proteins were completely demetalated after purification and then remetalated with Zn^{2+} (or with Co^{2+} for experiments involving UV−vis) also as previously described.[15] In this article, we did not remetalate SOD1 proteins with copper. The entire purification, demetalation, and zinc remetalation procedure was repeated twice to produce two separate batches of WT and two separate batches of A4V SOD1 proteins. Electrophoresis experiments used to assess the quaternary structure of SOD1 (described below) were performed repeatedly on both batches to exclude the possibility that the monomerization of A4V Zn_4−SOD1 in the electric field was the result of random experimental error or mishandling of protein solutions. The concentration of each SOD1 solution was measured by UV−vis spectroscopy using a molar extinction coefficient of 10 800 M^{-1} cm^{-1} at 280 nm. Metal content of apo- and Zn_4−SOD1 proteins was measured with inductively coupled plasma mass spectrometry (ICP-MS) as previously described.[15] All protein solutions were prepared using metal-free water (R = 18.2 MΩ, as dispensed from a Milli-Q filtration system), and all utensils were rinsed with 5 mM EDTA, followed by final rinsing with Milli-Q water.

DOI: 10.1021/acschemneuro.5b00146
ACS Chem. Neurosci. 2015, 6, 1696−1707

Protein Charge Ladders and Capillary Electrophoresis (CE). Each protein charge ladder was synthesized as previously described by acetylating Lys-ε-NH_3^+ in SOD1 with acetic anhydride to yield Lys-ε-$NHCOCH_3$.[15] In the case of Zn_4−SOD1, each ladder was prepared after titration of Zn^{2+} into apo-SOD1. The metal content of apo-SOD1 and Zn_4−SOD1 charge ladders was verified before and after acetylation with ICP-MS. Acetylation was performed by reacting protein solutions (buffered by 100 mM *N*-(2-hydroxyethy) piperazine-*N*′-(4-butanesulfonic acid), i.e., HEPBS, pH 9.0) with excess equivalents of acetic anhydride (diluted in neat 1,4-dioxane) at room temperature for 10 min. The acetylated protein was then transferred to 10 mM potassium phosphate buffer (for capillary electrophoresis) using centrifugal filtration. CE was performed in a bare fused silica capillary (60.2 cm in length) using a Beckman P/ACE system as previously described.[15] Electrophoresis was carried out at 5.0×10^4 V/m in 10 mM potassium phosphate buffer (pH 7.4); higher resolution CE was performed at 2.5×10^4 V/m. A constant temperature of 15 °C was maintained in the capillary with a liquid-cooled capillary jacket. Dimethylformamide (DMF) was added to each sample as an electrostatically neutral marker of electroosmotic flow. The mobility of each peak was calculated using the following equation:

$$\mu = \frac{L_D \cdot L_T}{V}\left(\frac{1}{t_{eof}} - \frac{1}{t}\right)$$

The electrophoretic mobility of each rung of the protein charge ladder was plotted versus its number of acetylated lysine residues in order to generate a plot from which the net charge of the protein could be determined as previously described.[15] The net charge of unmodified SOD1 protein can be calculated from a plot of electrophoretic mobility (of each rung of the charge ladder) against the number of acetylated lysines, as illustrated by the equation shown in Figure 3.

The external electric field that was used in this study was generated with the power source of the capillary electrophoresis instrument. Briefly, two solution wells were connected by a fused silica capillary that is 60.2 cm in length. A constant electric field was generated by applying a constant voltage (15 kV) with two platinum electrodes that were immersed into the glass reservoirs. An image of this apparatus is shown in Figure S4. Therefore, a constant electric field of 2.5×10^4 V/m in strength is generated. The measured current varied between 14 and 18 μA.

Differential Scanning Calorimetry (DSC). Experimental procedures used for DSC are described in previous reports.[15] Each protein sample was analyzed at a concentration of 2 mg/mL in 10 mM potassium phosphate buffer (pH 7.4). Thermal scanning occurred from 20−110 °C, at a scan rate of 1 °C/min.

Amide H/D Exchange in Absence and Presence of External Electric Field. For experiments in the absence of electric fields, each protein solution was transferred into 100 mM potassium phosphate buffer (pH 7.4) prior to amide H/D exchange, with a final concentration of ∼30 mg/mL. Hydrogen/deuterium exchange was initiated by diluting this concentrated protein solution into deuterium oxide (99.5% purity) at a 1:10 v/v ratio. Hydrogen/deuterium exchange was carried out at room temperature (23−25 °C) for 60 min. Prior to mass spectral analysis of each aliquot (at each time point), H/D exchange was quenched by flash freezing in liquid nitrogen (the time at which aliquots were frozen is the recorded time of the data point). Each protein solution was thawed by diluting with prechilled 0.3% formic acid (pH 2.5) followed by immediate injection into a desalting column coupled to the ESI-MS. The mobile phase of the desalting column was composed of 60% acetonitrile, 1.2% formic acid, and 38.8% Milli-Q water. The mass of eluted protein was measured using ESI-MS. At the end of the entire experiment, an aliquot of the protein solution was heated for 10 min with a PCR instrument at a temperature 5 °C below the T_m value to produce a perdeuterated protein sample. This sample was then used to quantify the rate of back exchange (D/H exchange) that occurred during ESI-MS analysis to accurately calculate the number of unexchanged hydrogens at each time point. The number of unexchanged hydrogens was calculated by subtracting the measured mass of the native protein in D_2O from the mass of the perdeuterated protein, as previously described.[15]

We also measured the rate of amide H/D exchange for various periods of time in A4V and WT Zn_4−SOD1 after exposure to an external electric field (15 kV/60.2 cm). Nonacetylated A4V and WT Zn_4−SOD1 (∼30 mg/mL) underwent H/D exchange as described above for 60 min to reach a plateau (i.e., to allow exchange of rapidly exchangeable amide NH's, leaving unexchanged NH's in the hydrophobic core of SOD1). H/D exchange was carried out in glass vials, wherein positive and negative electrodes from the CE instrument were immersed in one glass vial, and the two vials were connected via a 60.2 cm salt bridge of fused silica. Each vial contained an identical solution of SOD1 (250 μL, ∼3 mg/mL SOD1, pH 7.4) that was incubated in D_2O for 60 min prior to application of the electric field. Each protein solution was exposed to a 15 kV potential for 2−30 min at 23−25 °C before removal of a 10 μL aliquot and flash freezing of the aliquot for later mass spectral analysis (in triplicate). As a control, aliquots of the D_2O/SOD1 solution (10 μL) were also flash frozen and measured by ESI-MS after incubation at 23−25 °C (for 60 + 2−30 min) without exposure to the electric field. A microthermometer was used to measure the temperature of the glass vial containing the D_2O/SOD1 solution after 1−30 min at 15 kV (to quantify the degree of Joule heating). For these control experiments, the high voltage was switched off and the thermometer was immediately immersed in the D_2O/SOD1 solution (contained in a glass vial) in <45 s after voltage shut-off.

Theoretical Modeling of SOD1 Electrostatics. All calculations were performed using Discovery Studio 4.1, as described in Supporting Information.

■ ASSOCIATED CONTENT

Supporting Information

The Supporting Information is available free of charge on the ACS Publications website at DOI: 10.1021/acschemneuro.5b00146.

Additional experimental details and data (e.g., details of native iso-electric focusing and size exclusion chromatography, size exclusion chromatograms, capillary electropherograms, images of IEF gels, and tabulated charge and dipole values) (PDF).

■ AUTHOR INFORMATION

Corresponding Author

*E-mail: Bryan_Shaw@baylor.edu.

Author Contributions

†Y.S. and M.J.A. contributed equally in performing experiments and analyzing data.

Y.S., M.J.A., and B.F.S. participated in research design. All authors wrote the manuscript.

Funding

Financial support for this research was provided to B.F.S. by the Department of Defense (W81XWH-11-1-0790), the National Science Foundation (CHE: 1352122), and the Welch Foundation (AA-1854).

Notes

The authors declare no competing financial interest.

■ REFERENCES

(1) Lee, Y.-E. K., Smith, R., and Kopelman, R. (2009) Nanoparticle PEBBLE sensors in live cells and in vivo. *Annu. Rev. Anal. Chem. 2*, 57−76.

(2) Tyner, K. M., Kopelman, R., and Philbert, M. A. (2007) "Nanosized voltmeter" enables cellular-wide electric field mapping. *Biophys. J. 93*, 1163−1174.

DOI: 10.1021/acschemneuro.5b00146
ACS Chem. Neurosci. 2015, 6, 1696−1707

(3) Cunningham, J., Estrella, V., Lloyd, M., Gillies, R., Frieden, B. R., and Gatenby, R. (2012) Intracellular electric field and pH optimize protein localization and movement. *PLoS One 7*, e36894.
(4) Olivotto, M., Arcangeli, A., Carla, M., and Wanke, E. (1996) Electric fields at the plasma membrane level: a neglected element in the mechanisms of cell signalling. *BioEssays 18*, 495−504.
(5) Sakmann, B., and Neher, E. (1984) Patch clamp techniques for studying ionic channels in excitable membranes. *Annu. Rev. Physiol. 46*, 455−472.
(6) Zochowski, M., Wachowiak, M., Falk, C. X., Cohen, L. B., Lam, Y. W., Antic, S., and Zecevic, D. (2000) Imaging membrane potential with voltage-sensitive dyes. *Biol. Bull. 198*, 1−21.
(7) Ohtsuka, K., Sato, S., Sato, Y., Sota, K., Ohzawa, S., Matsuda, T., Takemoto, K., Takamune, N., Juskowiak, B., Nagai, T., and Takenaka, S. (2012) Fluorescence imaging of potassium ions in living cells using a fluorescent probe based on a thrombin binding aptamer-peptide conjugate. *Chem. Commun. 48*, 4740−4742.
(8) Zhou, X., Su, F., Gao, W., Tian, Y., Youngbull, C., Johnson, R. H., and Meldrum, D. R. (2011) Triazacryptand-based fluorescent sensors for extracellular and intracellular K+ sensing. *Biomaterials 32*, 8574−8583.
(9) Jensen, M. O., Jogini, V., Borhani, D. W., Leffler, A. E., Dror, R. O., and Shaw, D. E. (2012) Mechanism of voltage gating in potassium channels. *Science 336*, 229−233.
(10) Ojeda-May, P., and Garcia, M. E. (2010) Electric field-driven disruption of a native beta-sheet protein conformation and generation of a helix-structure. *Biophys. J. 99*, 595−599.
(11) Solomentsev, G. Y., English, N. J., and Mooney, D. A. (2010) Hydrogen bond perturbation in hen egg white lysozyme by external electromagnetic fields: a nonequilibrium molecular dynamics study. *J. Chem. Phys. 133*, 235102.
(12) Bekard, I., and Dunstan, D. E. (2014) Electric field induced changes in protein conformation. *Soft Matter 10*, 431−437.
(13) Freedman, K. J., Haq, S. R., Edel, J. B., Jemth, P., and Kim, M. J. (2013) Single molecule unfolding and stretching of protein domains inside a solid-state nanopore by electric field. *Sci. Rep. 3*, 1638.
(14) Shi, Y., Abdolvahabi, A., and Shaw, B. F. (2014) Protein charge ladders reveal that the net charge of ALS-linked superoxide dismutase can be different in sign and magnitude from predicted values. *Protein Sci. 23*, 1417−1433.
(15) Shi, Y., Mowery, R. A., and Shaw, B. F. (2013) Effect of metal loading and subcellular pH on net charge of superoxide dismutase-1. *J. Mol. Biol. 425*, 4388−4404.
(16) Chattopadhyay, M., and Valentine, J. S. (2009) Aggregation of copper-zinc superoxide dismutase in familial and sporadic ALS. *Antioxid. Redox Signaling 11*, 1603−1614.
(17) Inoue, E., Tano, K., Yoshii, H., Nakamura, J., Tada, S., Watanabe, M., Seki, M., and Enomoto, T. (2010) SOD1 Is Essential for the Viability of DT40 Cells and Nuclear SOD1 Functions as a Guardian of Genomic DNA. *J. Nucleic Acids 2010*, 795946.
(18) Della Valle, M. C., Sleat, D. E., Zheng, H., Moore, D. F., Jadot, M., and Lobel, P. (2011) Classification of subcellular location by comparative proteomic analysis of native and density-shifted lysosomes. *Mol. Cell. Proteomics 10*, M110.006403.
(19) Kawamata, H., and Manfredi, G. (2010) Import, maturation, and function of SOD1 and its copper chaperone CCS in the mitochondrial intermembrane space. *Antioxid. Redox Signaling 13*, 1375−1384.
(20) Galaleldeen, A., Strange, R. W., Whitson, L. J., Antonyuk, S. V., Narayana, N., Taylor, A. B., Schuermann, J. P., Holloway, S. P., Hasnain, S. S., and Hart, P. J. (2009) Structural and biophysical properties of metal-free pathogenic SOD1 mutants A4V and G93A. *Arch. Biochem. Biophys. 492*, 40−47.
(21) Sreedharan, J., and Brown, R. H. (2013) Amyotrophic lateral sclerosis: Problems and prospects. *Ann. Neurol. 74*, 309−316.
(22) Pratt, A. J., Shin, D. S., Merz, G. E., Rambo, R. P., Lancaster, W. A., Dyer, K. N., Borbat, P. P., Poole, F. L., 2nd, Adams, M. W., Freed, J. H., Crane, B. R., Tainer, J. A., and Getzoff, E. D. (2014) Aggregation propensities of superoxide dismutase G93 hotspot mutants mirror ALS clinical phenotypes. *Proc. Natl. Acad. Sci. U. S. A. 111*, E4568−E4576.
(23) Rotunno, M. S., and Bosco, D. A. (2013) An emerging role for misfolded wild-type SOD1 in sporadic ALS pathogenesis. *Front. Cell. Neurosci. 7*, 253.
(24) Chattopadhyay, M., Durazo, A., Sohn, S. H., Strong, C. D., Gralla, E. B., Whitelegge, J. P., and Valentine, J. S. (2008) Initiation and elongation in fibrillation of ALS-linked superoxide dismutase. *Proc. Natl. Acad. Sci. U. S. A. 105*, 18663−18668.
(25) Ding, F., and Dokholyan, N. V. (2008) Dynamical roles of metal ions and the disulfide bond in Cu, Zn superoxide dismutase folding and aggregation. *Proc. Natl. Acad. Sci. U. S. A. 105*, 19696−19701.
(26) Polymenidou, M., and Cleveland, D. W. (2011) The seeds of neurodegeneration: prion-like spreading in ALS. *Cell 147*, 498−508.
(27) Sugaya, K., and Nakano, I. (2014) Prognostic role of "prion-like propagation" in SOD1-linked familial ALS: an alternative view. *Front. Cell. Neurosci. 8*, 359.
(28) McAlary, L., Yerbury, J. J., and Aquilina, J. A. (2013) Glutathionylation potentiates benign superoxide dismutase 1 variants to the toxic forms associated with amyotrophic lateral sclerosis. *Sci. Rep. 3*, 3275.
(29) Svensson, A. E., Bilsel, O., Kayatekin, C., Adefusika, J. A., Zitzewitz, J. A., and Matthews, C. R. (2010) Metal-free ALS variants of dimeric human Cu,Zn-superoxide dismutase have enhanced populations of monomeric species. *PLoS One 5*, e10064.
(30) Lelie, H. L., Liba, A., Bourassa, M. W., Chattopadhyay, M., Chan, P. K., Gralla, E. B., Miller, L. M., Borchelt, D. R., Valentine, J. S., and Whitelegge, J. P. (2011) Copper and zinc metallation status of copper-zinc superoxide dismutase from amyotrophic lateral sclerosis transgenic mice. *J. Biol. Chem. 286*, 2795−2806.
(31) Arnesano, F., Banci, L., Bertini, I., Martinelli, M., Furukawa, Y., and O'Halloran, T. V. (2004) The unusually stable quaternary structure of human Cu,Zn-superoxide dismutase 1 is controlled by both metal occupancy and disulfide status. *J. Biol. Chem. 279*, 47998−48003.
(32) Doucette, P. A., Whitson, L. J., Cao, X., Schirf, V., Demeler, B., Valentine, J. S., Hansen, J. C., and Hart, P. J. (2004) Dissociation of human copper-zinc superoxide dismutase dimers using chaotrope and reductant. Insights into the molecular basis for dimer stability. *J. Biol. Chem. 279*, 54558−54566.
(33) Kayatekin, C., Zitzewitz, J. A., and Matthews, C. R. (2010) Disulfide-Reduced ALS Variants of Cu, Zn Superoxide Dismutase Exhibit Increased Populations of Unfolded Species. *J. Mol. Biol. 398*, 320−331.
(34) Baker, E. G., Bartlett, G. J., Crump, M. P., Sessions, R. B., Linden, N., Faul, C. F., and Woolfson, D. N. (2015) Local and macroscopic electrostatic interactions in single alpha-helices. *Nat. Chem. Biol. 11*, 221−228.
(35) Hol, W. G., van Duijnen, P. T., and Berendsen, H. J. (1978) The alpha-helix dipole and the properties of proteins. *Nature 273*, 443−446.
(36) Gitlin, I., Carbeck, J. D., and Whitesides, G. M. (2006) Why are proteins charged? Networks of charge-charge interactions in proteins measured by charge ladders and capillary electrophoresis. *Angew. Chem., Int. Ed. 45*, 3022−3060.
(37) Goto, J. J., Zhu, H., Sanchez, R. J., Nersissian, A., Gralla, E. B., Valentine, J. S., and Cabelli, D. E. (2000) Loss of in vitro metal ion binding specificity in mutant copper-zinc superoxide dismutases associated with familial amyotrophic lateral sclerosis. *J. Biol. Chem. 275*, 1007−1014.
(38) Abdolvahabi, A., Shi, Y., Rhodes, N. R., Cook, N. P., Marti, A. A., and Shaw, B. F. (2015) Arresting amyloid with coulomb's law: acetylation of ALS-linked SOD1 by aspirin impedes aggregation. *Biophys. J. 108*, 1199−1212.
(39) Abdolvahabi, A., Gober, J. L., Mowery, R. A., Shi, Y., and Shaw, B. F. (2014) Metal-ion-specific screening of charge effects in protein amide H/D exchange and the Hofmeister series. *Anal. Chem. 86*, 10303−10310.

DOI: 10.1021/acschemneuro.5b00146
ACS Chem. Neurosci. 2015, 6, 1696−1707

(40) Shaw, B. F., Arthanari, H., Narovlyansky, M., Durazo, A., Frueh, D. P., Pollastri, M. P., Lee, A., Bilgicer, B., Gygi, S. P., Wagner, G., and Whitesides, G. M. (2010) Neutralizing positive charges at the surface of a protein lowers its rate of amide hydrogen exchange without altering its structure or increasing its thermostability. *J. Am. Chem. Soc. 132*, 17411−17425.
(41) Hough, M. A., Grossmann, J. G., Antonyuk, S. V., Strange, R. W., Doucette, P. A., Rodriguez, J. A., Whitson, L. J., Hart, P. J., Hayward, L. J., Valentine, J. S., and Hasnain, S. S. (2004) Dimer destabilization in superoxide dismutase may result in disease-causing properties: Structures of motor neuron disease mutants. *Proc. Natl. Acad. Sci. U. S. A. 101*, 5976−5981.
(42) Strange, R. W., Antonyuk, S. V., Hough, M. A., Doucette, P. A., Valentine, J. S., and Hasnain, S. S. (2006) Variable metallation of human superoxide dismutase: atomic resolution crystal structures of Cu-Zn, Zn-Zn and as-isolated wild-type enzymes. *J. Mol. Biol. 356*, 1152−1162.
(43) Furukawa, Y., and O'Halloran, T. V. (2005) Amyotrophic lateral sclerosis mutations have the greatest destabilizing effect on the apo- and reduced form of SOD1, leading to unfolding and oxidative aggregation. *J. Biol. Chem. 280*, 17266−17274.
(44) Hong, P., Koza, S., and Bouvier, E. S. (2012) Size-Exclusion Chromatography for the Analysis of Protein Biotherapeutics and their Aggregates. *J. Liq. Chromatogr. Relat. Technol. 35*, 2923−2950.
(45) Shaw, B. F., Durazo, A., Nersissian, A. M., Whitelegge, J. P., Faull, K. F., and Valentine, J. S. (2006) Local unfolding in a destabilized, pathogenic variant of superoxide dismutase 1 observed with H/D exchange and mass spectrometry. *J. Biol. Chem. 281*, 18167−18176.
(46) Rodriguez, J. A., Shaw, B. F., Durazo, A., Sohn, S. H., Doucette, P. A., Nersissian, A. M., Faull, K. F., Eggers, D. K., Tiwari, A., Hayward, L. J., and Valentine, J. S. (2005) Destabilization of apoprotein is insufficient to explain Cu,Zn-superoxide dismutase-linked ALS pathogenesis. *Proc. Natl. Acad. Sci. U. S. A. 102*, 10516−10521.
(47) Shi, Y., Rhodes, N. R., Abdolvahabi, A., Kohn, T., Cook, N. P., Marti, A. A., and Shaw, B. F. (2013) Deamidation of asparagine to aspartate destabilizes Cu, Zn superoxide dismutase, accelerates fibrillization, and mirrors ALS-linked mutations. *J. Am. Chem. Soc. 135*, 15897−15908.
(48) Saeed, M., Yang, Y., Deng, H. X., Hung, W. Y., Siddique, N., Dellefave, L., Gellera, C., Andersen, P. M., and Siddique, T. (2009) Age and founder effect of SOD1 A4V mutation causing ALS. *Neurology 72*, 1634−1639.
(49) Prudencio, M., Hart, P. J., Borchelt, D. R., and Andersen, P. M. (2009) Variation in aggregation propensities among ALS-associated variants of SOD1: correlation to human disease. *Hum. Mol. Genet. 18*, 3217−3226.
(50) Fried, S. D., Bagchi, S., and Boxer, S. G. (2014) Extreme electric fields power catalysis in the active site of ketosteroid isomerase. *Science 346*, 1510−1514.
(51) Chen, L. B. (1988) Mitochondrial membrane potential in living cells. *Annu. Rev. Cell Biol. 4*, 155−181.
(52) Meehan, C. F., Moldovan, M., Marklund, S. L., Graffmo, K. S., Nielsen, J. B., and Hultborn, H. (2010) Intrinsic properties of lumbar motor neurones in the adult G127insTGGG superoxide dismutase-1 mutant mouse in vivo: evidence for increased persistent inward currents. *Acta Physiol. 200*, 361−376.
(53) Cozzolino, M., Rossi, S., Mirra, A., and Carri, M. T. (2015) Mitochondrial dynamism and the pathogenesis of Amyotrophic Lateral Sclerosis. *Front. Cell. Neurosci. 9*, 31.
(54) Tan, W., Pasinelli, P., and Trotti, D. (2014) Role of mitochondria in mutant SOD1 linked amyotrophic lateral sclerosis. *Biochim. Biophys. Acta, Mol. Basis Dis. 1842*, 1295−1301.
(55) Vijayvergiya, C., Beal, M. F., Buck, J., and Manfredi, G. (2005) Mutant superoxide dismutase 1 forms aggregates in the brain mitochondrial matrix of amyotrophic lateral sclerosis mice. *J. Neurosci. 25*, 2463−2470.
(56) Kong, J., and Xu, Z. S. (1998) Massive mitochondrial degeneration in motor neurons triggers the onset of amyotrophic lateral sclerosis in mice expressing a mutant SOD1. *J. Neurosci. 18*, 3241−3250.
(57) Eddy, M. T., Andreas, L., Teijido, O., Su, Y., Clark, L., Noskov, S. Y., Wagner, G., Rostovtseva, T. K., and Griffin, R. G. (2015) Magic angle spinning nuclear magnetic resonance characterization of voltage-dependent anion channel gating in two-dimensional lipid crystalline bilayers. *Biochemistry 54*, 994−1005.

DOI: 10.1021/acschemneuro.5b00146
ACS Chem. Neurosci. 2015, 6, 1696−1707